Polymer Chemistry

Controlling Network Morphology in Hybrid Radical/Cationic Photopolymerized Systems

Journal:	*Polymer Chemistry*
Manuscript ID	PY-ART-10-2022-001288.R1
Article Type:	Paper
Date Submitted by the Author:	10-Nov-2022
Complete List of Authors:	Grover, Tanner; The University of Iowa, Chemical and Biochemical Engineering Guymon, C.; The University of Iowa, Chemical and Biochemical Engineering

Controlling Network Morphology in Hybrid Radical/Cationic Photopolymerized Systems

Tanner L. Grover[a] and C. Allan Guymon[a,*]
[a]Department of Chemical and Biochemical Engineering, University of Iowa, 4133 Seamans Center, Iowa City, IA 52242, USA
*Corresponding Author: allan-guymon@uiowa.edu

Abstract

Controlling phase separation during radical/cationic hybrid photopolymerization may provide a method for manipulating polymer morphology and material properties of photocured networks. However, regulating phase separation during the highly dynamic cross-linking process remains challenging. In this study, we combined a cationic oxetane/epoxide comonomer system with a methacrylate resin to examine the effects of the cationic comonomer ratio on reaction kinetics, network morphology, and bulk material properties. At high loadings of oxetane, the dissimilar reaction rates between the rapid free-radical and relatively slow cationic photopolymerization led to highly phase separated structures. Conversely, small additions of epoxide significantly accelerated the cationic polymerization enabling control over the rate difference between hybrid photopolymerizations. Ultimately, modifications to the comonomer ratio enabled substantial control over kinetics and polymer structure. When the dual photopolymerizations occurred on similar time scales, greater network interpenetration was exhibited, whereas increased phase separation was induced with more sequential polymerizations. This ability to control polymer structure through comonomer content permits a broad range of tailorable mechanical properties for photocured films. Notably, although photopolymer tensile strength and elongation can be adapted, tensile toughness is maintained across a wide array of phase separated morphologies and is significantly improved relative to the neat methacrylate network. Finally, these systems were incorporated in 3D constructs using stereolithography, demonstrating that decreased phase separation size-scale enables greater impact strength of 3D printed objects. The results of this work show that internally regulating cationic polymerization rate using comonomer composition provides control over polymer structure and material properties in radical/cationic photopolymer systems.

1 Introduction

Photopolymerization of cross-linking monomers to form in situ polymer networks with high stiffness and solvent resistance has become an attractive technology for applications such as protective coatings, adhesives, biomedical materials, and 3D printing.[1–4] Free-radical polymerization of (meth)acrylate monomers is commonly used in photopolymerization due to inherent fast reaction rates which allows for rapid material production. However, low mechanical resiliency, which is largely dependent on polymer structure, limits the application and expansion of photopolymers as engineering materials.[5] Fast reaction rates through chain growth mechanisms lead to gelation at early stages in the reaction and create exceedingly irregular network structure accompanied with high degrees of internal stress.[5] These irregularities can be attributed to the formation during network evolution of nano/microgels which contain high internal cross-link density and relatively low covalent connectivity.[6] The low connectivity manifests through bulk material properties with fracture prone pathways that increase material failure rates in high stress applications.[7] To overcome these challenges, considerable attention has been focused on directing polymer structure to ultimately control the macroscopic properties of photocured materials.

Significant work has focused on exploring alternative photopolymerization-compatible chemistries to produce materials with greater functionality and mechanical resilience. Methods such as molecular templating, controlled radical polymerization, and nanoparticle inclusion have shown promise in tuning photopolymer architecture to produce unique properties.[8–12] Particularly, simultaneous hybrid/orthogonal photopolymerizations, e.g., mixtures of cationic and free-radical monomers, have produced composites with various morphologies ranging from interpenetrating polymer networks (IPNs) to photopolymerization-induced phase separated (PhIPS) materials.[13–16] IPNs are produced with at least two highly entangled polymer networks that are not chemically connected. IPNs may be formed through the simultaneous polymerization of orthogonal reactions and display little to no evident phase

separation due to compatibility throughout the cross-linking process.[17] Conversely, although PhIPS networks incorporate multiple polymers, distinct regions or phases ranging from the nano- to macroscale develop with substantially different composition.[18,19] The domain morphology and size scale is determined by the competition between phase separation and the polymerization kinetics during network evolution.[20] The fast reaction kinetics afforded by photopolymerization, in contrast to other polymerization processes, provide the distinct advantage of regulating the degree of phase separation by kinetically entrapping morphologies before spinodal decomposition.[21,22] Therefore, by manipulating chemical and physical parameters during photopolymerization, it may be possible to control intraphase structure, size, composition, and interphase connectivity to tailor photopolymer performance.

Previous work has demonstrated that substantial influence over polymer morphology can be achieved by varying comonomer concentrations.[23] de With and coworkers examined the effects of comonomer concentration of a (meth)acrylate/epoxide system on phase miscibility before and after photopolymerization. Interestingly, their findings suggest that miscibility of the monomeric solution predicts dual phase development in the polymeric state and that monomer solubility parameters can be used to predict phase separated morphologies.[24] Additionally, photopolymerization kinetics also play a large role in dual phase development.[25] Recent results have demonstrated that increased initiating light intensity significantly alters the reaction kinetics and resulting morphology of an oxetane/acrylate hybrid resin.[21] At relatively low light intensities, the initiation and subsequent polymerization of acrylate species is much faster than the oxetane homopolymerization. Therefore, the acrylate polymer develops and begins to phase separate from the monomeric oxetane during photopolymerization. By increasing light intensity, the differences in polymerization rate are greatly reduced, and the two networks form at more similar rates. The simultaneous evolution of both networks reduces macromolecule diffusion and phase separation which results in greater interpenetration between networks. The retention of dual

phases in combination with greater interconnectivity was shown to produce materials with significantly improved toughness relative to a highly phase separated structure.

While dual phase materials can be prepared by taking advantage of the dissimilar reaction kinetics in hybrid photopolymerizations, the manipulation of external stimuli such as light intensity can be limited in applications such as 3D printing. Therefore, it is important to investigate chemistries that can endogenously control reaction rate differences in hybrid systems independent of external parameters. One such system that may allow rate changes without changing light intensity incorporates epoxides in oxetane cationic photopolymerization. Crivello and coworkers have shown that the onset of oxetane polymerization can be finely tuned through copolymerization with epoxide-bearing monomers.[26] Homo-photopolymerization of oxetane often results in a delayed polymerization onset and low final monomer conversion due to the relatively high energy barrier for the four-membered ring opening.[27] However, when oxetane is polymerized in the presence of epoxide, the higher-ring strain epoxide rapidly produces oxiranium ions that can promote ring-opening and enhanced reactivity of oxetane through copolymerization.[26,28] Additionally, onset of photopolymerization and rate can be controlled by tuning the comonomer ratio. Thereby, it may be possible to precisely regulate the cationic reaction in a hybrid polymerization and manipulate differences in the development of free-radical and cationic polymerizing networks.

In this work, we investigated the effects of the oxetane/epoxide comonomer ratio on reaction kinetics and network morphology in a hybrid photopolymerizable system. A mono-oxetane and di-epoxide, the cationic monomer system, were incorporated into a methacrylate resin. The ratio of oxetane to epoxide was varied to accelerate the cationic photopolymerization and control the onset and domain evolution in relation to the free-radical based network. Functional group conversions during photopolymerization were monitored individually using real-time infrared spectroscopy to determine differences in free-radical and cationic photopolymerization rate and conversion. Dynamic mechanical

analysis was used to measure the tan δ of hybrid networks and provide details regarding individual phase and bulk thermomechanical properties. Photopolymer morphology information such as relative phase size, interconnectivity, and relative moduli was characterized using atomic force microscopy. Tensile testing was used to correlate polymer structure with bulk properties and illustrate the impact of domain morphology on mechanical performance. Additionally, hybrid formulations were polymerized using stereolithography to investigate the impact of internal control over phase morphology in 3D photopolymerization. This research thereby aims to show that photopolymer structure and bulk properties can be controlled using monomer composition and reaction kinetics in hybrid polymerizations.

2 Materials and Methods

2.1 Materials

The hybrid photopolymerizable system investigated was a formulation of orthogonally polymerizable monomers. 40 wt% of the formulation consisted of monomers incorporating cyclic ethers that polymerize through cationic mechanisms while the remaining 60 wt% of the formulation consisted of methacrylates that undergo free-radical polymerization. The cationic formulation for study contained various ratios of monooxetane, 3-ethyl-3-[(2-ethylhexyloxy)methyl] oxetane (EHOX, Toagosei), and diepoxide, 3,4-epoxycyclohexylmethyl 3,4-epoxycyclohexanecarboxylate (EEC, Sigma). The free-radical portion of the system was comprised of 60 wt% bisphenol A ethoxylated methacrylate (BisEMA, SR540, Sartomer) and 40 wt% hydroxyethyl methacrylate (HEMA, Sigma). The hydroxyl group on HEMA can participate in cationic polymerization enabling covalent bonding between the two networks thereby increasing compatibility. Figure 1 shows the chemical structures of the monomers used while Table 1 lists cationic comonomer compositions examined. The cationic photoinitiator and photosensitizer used were 2.0 wt% triarylsulfonium hexafluoroantimonate salts (TSA, 50 wt% in propylene carbonate, Sigma),

and 2.0 wt% isopropyl thioxanthone (ITX, Irgacure), respectively. 0.10 wt% phenylbis(2,4,6-trimethylbenzoyl)phosphine oxide (BAPO, Ciba) was added as a radical photoinitiator, and 0.17 wt% 2,5-Bis(5-tert-butyl-benzoxazol-2-yl)thiophene (Sigma) was incorporated as a light blocker for 3D printing resolution. Concentrations of photoactive species were based on the total monomeric formulation. All chemicals were used as received.

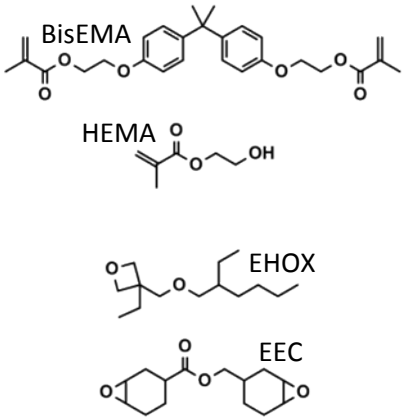

Figure 1. Chemical structures of free-radical polymerizable monomers, BisEMA and HEMA, and cationic polymerizable monomers, EHOX and EEC.

Table 1. Cationic monomer weight ratio in hybrid resin[a]

Formulation	EHOX	EEC
100O-0E	100	0
75O-25E	75	25
60O-40E	60	40
50O-50E	50	50
0O-100E	0	100

[a]All formulations contain 60 wt% free-radical and 40 wt% cationic monomers based on the ratios in Table 1.

2.2 Methods

Photopolymerization Kinetics. Real-time Fourier transform infrared spectroscopy (RT-IR) was used to monitor peak area of the absorption bands for methacrylate (1642-1631 cm^{-1})[29], oxetane (987-976 cm^{-1}),[28] and epoxide (793-775 cm^{-1})[28] functional groups during photocuring. 10 µL samples were placed between two NaCl plates and mounted on a horizontal stage for an RT-IR spectrometer (Nexus 670, Thermo-Nicolet). Samples were illuminated with a mercury arc lamp (1500 Series, Omnicure) equipped with a 400-500 nm band pass filter at an incident light intensity of 20 mW/cm^2. Data collection preceded illumination by 30 seconds to ensure a stable baseline. Fractional conversion as a function of time was determined by dividing the instantaneous peak area by the initial peak area.[21]

Dynamic Mechanical Analysis. Thermomechanical and phase behavior of cured films were examined using a dynamic mechanical analyzer (DMA Q800, TA Instruments). Polymer films were prepared by placing liquid samples between glass slides separated using 150 µm spacers. The samples were then exposed to a 405 nm light (LED Spot 100 IC, Honle) at an incident intensity of 20 mW/cm^2 for 5 minutes. After photocuring, Samples were thermally post-cured for 2 hours at 150°C and then cut into strips to yield 12 mm x 2 mm bars. The loss factor (tan δ) was measured using DMA in frequency sweep mode with a frequency of 1 Hz and an oscillation amplitude of 15 µm while ramping temperature from -60°C to 150°C. Here, the maxima of the tan δ versus temperature curves are reported as the domain glass transition temperature.[30]

Atomic Force Microscopy. Surface morphology of polymer films were probed using an atomic force microscope (AFM, MFP-3D, Asylum Research) in tapping mode. Sample were prepared by coating a glass slide with the liquid formulation and exposing to a 405 nm LED at 20 mW/cm^2 for 5 minutes under an N_2 atmosphere. After photocuring, samples were thermally post-cured for 2 hours at 150°C. Phase images were obtained by linearly scanning an oscillating nano-sized probe (SPM Probe, MikroMasch) across the polymer surface at a tapping rate of 1 Hz.[21] The interaction between the probe and material is measured by a change in oscillation/phase angle. Output data was processed using Igor software (WaveMetrics).

Tensile Property Analysis. Bulk mechanical properties were determined using the same sample preparation and instrument as the dynamic mechanical analysis experiments. For stress-strain analysis, samples were clamped in a DMA tensile fixture and subjected to an increasing load at a constant force rate of 2 N/min until material failure. Tensile modulus was determined using the initial slope (< 0.1% strain) of the stress/strain curve. Ultimate tensile strength and elongation is noted at the point of material failure, and toughness was calculated by area under stress-strain curve. Creep testing was used to examine deformation behavior before and after sudden load. For creep analysis tensile bars were subjected to an instantaneous stress of 10 MPa. This level of force was maintained for 10 minutes and then released. The deformation behavior was monitored continuously as a function of time.

3D Printing and Impact Testing. A modified DLP 3D printer (Ember, Autodesk) was used to construct stereolithography working curves for the hybrid formulations and print Izod impacts test specimens. A panel composed of 10 distinct squares was printed by exposing a filled resin vat with a transparent FEP window to a 405 nm LED projector at 20 mW/cm^2. Each spatially resolved square was subjected to a different light dose and the resulting cure depth of each square was measured using a micrometer (Mitutoyo). A linear model was used to fit cure depth versus light dose where the slope is related to the light absorptivity of the resin and the x-intercept is equal to the energy needed to induce macro-gelation at the resin surface.[31] Izod-notched impact blocks with dimensions of 40 x 10 x 6.25 mm^3 (L·W·D), notch

radius of 1 mm, and notch depth of 0.5 mm were constructed using CAD software (Fusion 360, Autodesk). CAD models were sliced into 25 µm thick layers using 3D printing software (Print Studio, Autodesk). Printing was performed with 8 seconds of light exposure per layer. Impact blocks were post-cured for 2 hours at 150°C. Impact testing was performed with a 1 J pendulum impact tester (HIT5.5P, Zwick/Roell) with the direction of impact energy perpendicular to layer lamination.

3 Results and Discussion

Prior studies have shown that the reactivity and induction period of oxetane photopolymerization can be endogenously regulated by the presence and relative concentration of an epoxy comonomer. Therefore, in a simultaneous cationic and free-radical polymerization, using epoxy to change the onset of cationic polymerization and thereby the inherent time scales of network formation may allow control of phase separation between both systems and ultimately material properties. Combining orthogonal polymerizations while regulating phase separation can lead to enhanced properties relative to the neat homopolymer networks, e.g. toughness, surface hardness, and shrinkage.[32,33] These changes may be attributed to the incorporation of domains that impart desirable and synergistic characteristics for ultimate material performance. This work focuses on manipulating cationic polymerization kinetics in cationic/free-radical hybrid systems to control network evolution and the resulting polymer network morphology. We hypothesize that altering the cationic comonomer ratio will enable control of the degree of dual network interpenetration and will induce significant changes in mechanical properties of these photopolymerized materials.

Reaction kinetics directly impact the resulting morphology through phase separation processes. To determine the range of kinetic behavior that could be used to control morphology in these hybrid systems, photopolymerization kinetics were examined. Figure 2A-C compares the real-time reactive group conversion of methacrylate, oxetane, and epoxide functional groups, respectively, for hybrid

polymerizations with varying ratios of EHOX to EEC (epoxide monomer). Independent of cationic monomer content, the free-radical polymerization initiates almost instantaneously when exposed to light (Fig 2A). Conversely, in the absence of EEC (Fig 2B, 100O-0E) very little oxetane conversion (~5%) is achieved even after 10 minutes while only reaching 40% conversion after 30 minutes of light exposure. With this large disparity between the orthogonal polymerizations, the free-radical reaction establishes polymer structure and possibly phase separates well before any significant cationic polymerization occurs. Additionally, this material qualitatively exhibited macroscopic phase-separated characteristics such as optical opacity and brittleness[34] providing further evidence that the differences in reaction rate have significant impact on polymer morphology. Included in the supplementary information are digital images showing the presence of opacity post photopolymerization (S.1-2) indicating that phase separated structures are induced during light irradiation.

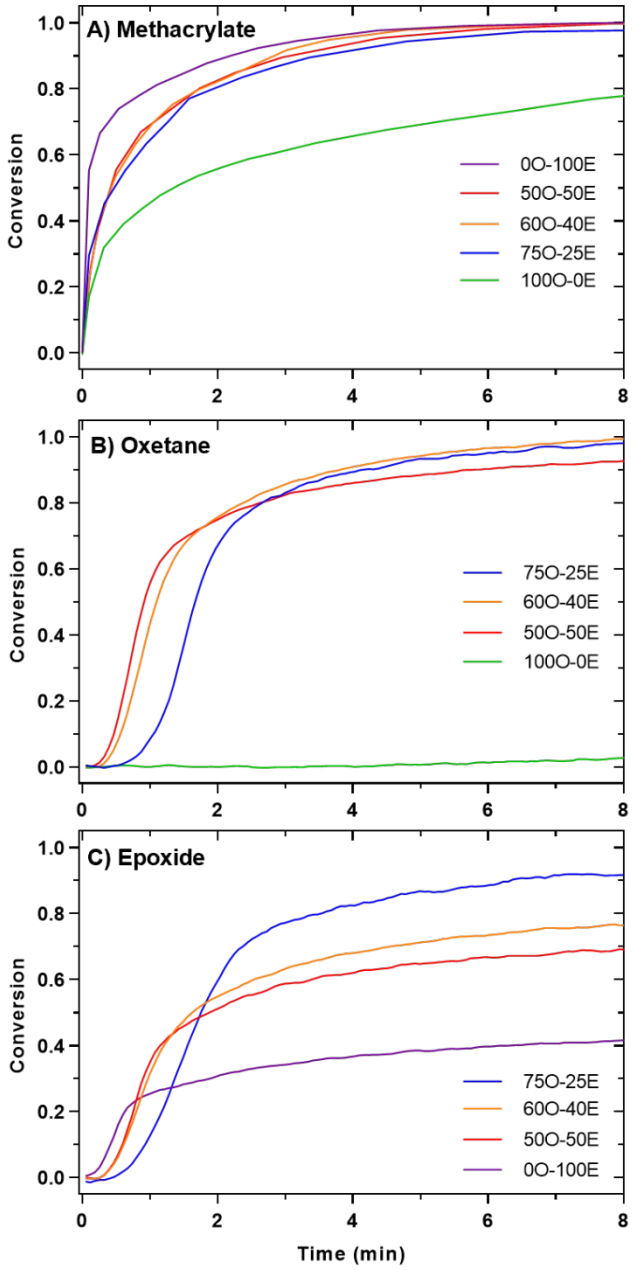

Figure 2A-C. Conversion as a function of time for (A) methacrylate, (B) oxetane, and (C) epoxide functional groups during hybrid photopolymerizations. All formulations contained 60 wt% free-radical and 40 wt% cationic polymerizing monomers. The weight fraction of the two cationic monomers in the cationic portion was varied as denoted in the plot legends. Respective peak areas for methacrylate, oxetane, and epoxide functional groups were monitored using RT-FTIR. Samples were cured using 400-500 nm light at 20 mW/cm^2.

The large time scale differences in kinetics between the free-radical and cationic polymerization can be reduced by accelerating the oxetane polymerization through the inclusion of epoxide. Upon the addition of EEC, i.e., the 75O-25E formulation in Figure 2B, the polymerization onset of EHOX occurs in

less than 40 seconds of light exposure and reaches greater than 90% conversion within five minutes. Furthermore, the EHOX induction period is progressively reduced by increasing EEC content. The onset of polymerization for the 60O-40E and 50O-50E formulations occurs at approximately 30 seconds and 20 seconds of light exposure, respectively, showing that the time difference between polymerizations is controllable through comonomer composition. The reduced induction time leads to more simultaneous polymerization of the separate cationic and free-radical reactions thus potentially altering the size scale of phase separation. The combination of these two monomers also influences the epoxide conversion. As the EHOX-EEC ratio is increased, considerably higher conversions for epoxide groups are observed as shown in Figure 2C. The increase in conversion may be due to the epoxide co-propagating within a less viscous oxetane phase as opposed to the reaction occurring in an already highly cross-linked and vitrified methacrylate network. As the cationic domain becomes more cross-linked with greater EEC concentration, the ultimate epoxide conversion decreases and only reaches 40 % conversion when no EHOX is present, i.e., the 0O-100E system. Moreover, the addition of EEC enhances methacrylate polymerization rate which likely stems from the higher reactivity of the epoxide functional group relative to oxetane. The faster reaction in the cationic domain generates additional heat in the system increasing temperature and thereby increasing the speed of the methacrylate reaction.[35]

Controlling the induction period of the EHOX polymerization with epoxide addition may change phase separated morphology and enable control over polymer structure. To determine the effect of reaction kinetics and oxetane/epoxide composition on structural morphology, thermomechanical behavior of photopolymerized hybrid materials was determined using dynamic mechanical analysis (DMA). In DMA, a stress is applied to the material which is either stored or dissipated as heat with the ratio of dissipated to stored energy defined as the tan δ.[36] Tan δ behavior is highly dependent on temperature due to accessible molecular configurations. As temperature is increased, greater molecular motions are accessible, and macromolecular rearrangements can occur allowing greater dissipation.

Hence, a less cross-linked material will exhibit increased dissipation of energy at lower temperatures due to the greater ability to deform under an applied stress.

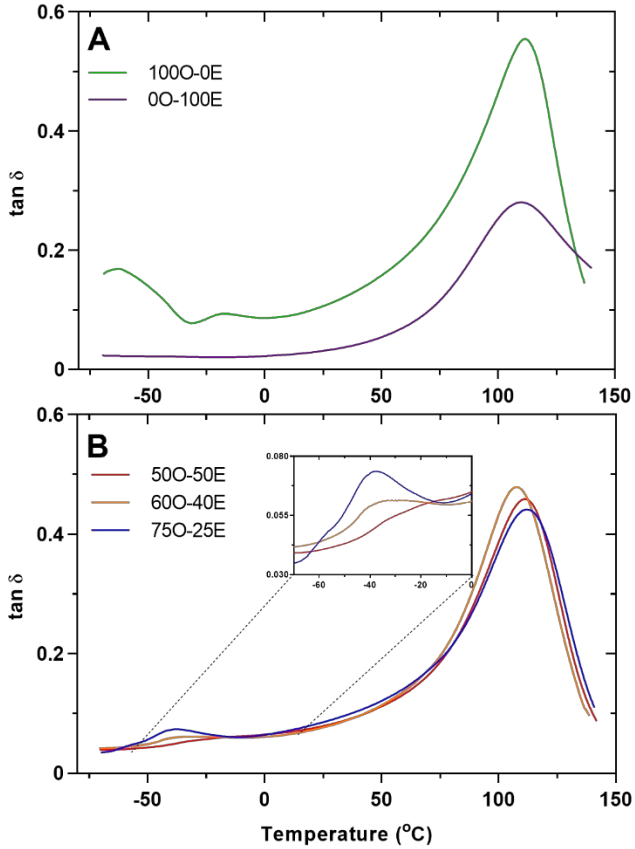

Figure 3A-B. Tan δ versus temperature for hybrid photopolymer systems containing (A) only one cationic monomer and (B) mixtures of cationic comonomers. All formulations contained 60 wt% free-radical and 40 wt% cationic polymerizing monomers. Polymer films were fabricated by photocuring for 5 minutes using a 405 nm LED at 20 mW/cm^2 and then thermally post curing at 150°C for 2 hrs. Samples were subjected to an oscillating strain (1 Hz) at an amplitude of 15 µm while ramping temperature.

Shown in Figure 3A are tan δ profiles for hybrid materials that contain only one cationic monomer in the formulation. When no epoxide is present in the system, 100O-0E, the material displays two distinct maxima corresponding to regions of considerably different domain structure. The high temperature maximum is likely due to a highly cross-linked, primarily methacrylate domain which has a glass transition temperature greater than 100°C. The maximum below -50°C is likely due to EHOX rich domains that, due to low cross-link density, allow greater translational motion and are only glassy at very low temperatures. The presence of two maxima suggests phase separated morphology within the

bulk material coming from distinctly different structural environments in each domain. The phase separated behavior is consistent with the considerably different rates of photopolymerization for the free-radical and cationic networks. As shown in the kinetics experiments, the free-radical polymerization is much faster implying that the methacrylate network propagates much more rapidly than the cationic polymer and phase separates from the oxetane monomer rich matrix. On the other hand, when only EEC is present (0O-100E) the two polymer networks develop on similar time scales which significantly reduces diffusion and phase separation from occurring. Therefore, greater integration and interpenetration between networks is observed as represented by the single thermal transition in the 0O-100E tan delta plot.

The position and magnitude of the low temperature tan δ maximum can be altered depending on the epoxide content as shown in Figure 3B. Increasing the epoxide concentration induces a reduction in relative peak height and shift to higher temperatures. It should be noted that inclusion of EEC can change domain properties in addition to photopolymerization rate effects. Since EEC contains two reactive epoxide groups, the addition of EEC increases the cross-link density of the cationic domain. Therefore, in addition to enhanced polymerization kinetics, the physical presence of a more cross-linked cationic domain can limit diffusion and phase segregation between the two orthogonal polymerizations. Additionally, as the cationic domain becomes more cross-linked with increasing EEC, chain rearrangements are impeded, increasing storage modulus. Therefore, the disappearance of the low temperature maximum stems not only from increasing interpenetration but also from a stiffer cationic network.

Significant evidence of different phase separation with various ratios of cationic monomers is observed from tan delta peaks. To determine how these changes manifest spatially in bulk morphology, atomic force microscopy (AFM) phase imaging was used. In AFM, a nano-sized probe with a radius of curvature on the atomic level is oscillated and tapped across a sample surface. The interaction between

the probe and material is then measured by a change in oscillation/phase angle. When the probe interacts with a relatively low modulus material, the phase angle will increase due to the material allowing greater deformation. In contrast, materials with a high modulus will show reduced phase angle stemming from a more elastic interaction.[37] Figure 4 shows the AFM phase images for the hybrid formulations containing mixtures of EHOX and EEC after photopolymerization and thermal post cure. At low EEC concentration (Fig 4, 75O-25E), which provides the greatest evidence of dual phase formation from tan δ results, the two domains are distinct and clearly visible. The cationic domain containing relatively low cross-linking is represented by a high phase angle and is relatively continuous through the material. On the other hand, the high modulus domain from densely cross-linked (meth)acrylate, corresponding to the low phase angle, is comparatively discontinuous with low connectivity between localized regions. Additionally, the steep gradient between domains illustrates minimal entanglements at the phase interface and confirms high degrees of separation between the two domains.

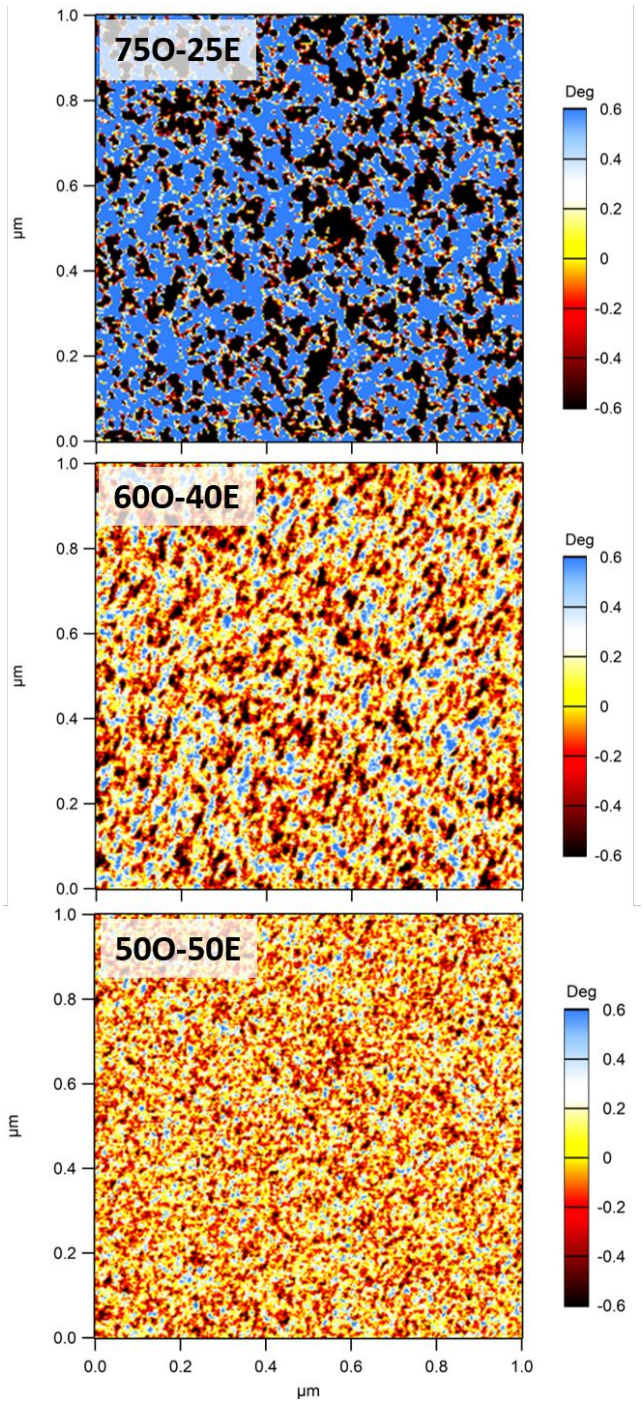

Figure 4. Atomic force microscopy phase images of hybrid polymer networks at varied oxetane to epoxide ratios (75O-25E, 60O-40E, and 50O-50E) as denoted in each image. All formulations contained 60 wt% free-radical and 40 wt% cationic polymerizing monomers. Samples were prepared by exposing liquid formulations to 405 nm LED at 20 mW/cm^2 for 5 minutes and then thermally post cured at 150°C for 2 hrs. The degree scale corresponds to a change in oscillation frequency of the probe due to material modulus.

With further increases in epoxide content, considerable integration of the orthogonal networks is evident (Fig 4, 60O-40E). At this ratio, a much more pronounced tertiary domain (i.e., interphase) develops in addition to the domains correlating to the primarily radical and cationic orthogonal networks. This interphase corresponds to a mixture with both free-radical and cationic derived networks with high levels of entanglement as indicated by the gradual change in phase angle. In contrast to the 75O-25E material, the 60O-40E morphology can be attributed to both polymerizations producing networks at similar rates which restricts macromolecule diffusion and spinodal decomposition thus leading to greater interpenetration. Also, the greater EEC content increases cross-linking and modulus in the cationic domain which decreases the phase angle. At the 50O-50E ratio, the two phases are nearly indistinguishable, exhibiting a relatively homogenous structure. Since both polymerizations are occurring on nearly the same time scale, the two networks are forming simultaneously which results in near-IPN like structure. As a control, AFM phase images were obtained prior to thermal post cure to confirm phase separation and basic polymer morphology were induced during photopolymerization and not during thermal post cure. As shown in Figure S.3, phase separation is apparent post photopolymerization with decreasing domain size scales with higher EEC loadings. Ultimately, the ability to regulate reaction rate and cross-linking in the cationic phase provides a method for tailoring the structure of the material which may considerably influence material performance.

Due to the large changes in kinetics and material morphology, it is likely that considerable differences in mechanical properties will also be observed. Additionally, composites formed with localized regions of differing chemical composition and strong interfacial adhesion do exhibit unique properties relative to their neat components.[38] To determine if materials properties are influenced by composition and morphology, creep behavior was determined for these hybrid networks to understand the interplay between relative domain size, interconnectivity, and cross-link density (Fig. 5). Creep testing involves applying an instantaneous and constant load to the material and measuring resulting

elongation.[30] In highly cross-linked polymers, molecular rearrangement is highly restricted due to the covalent linkages between chains. This rearrangement limitation is apparent for the formulation with the highest epoxide loading, 50O-50E, which displays very little elongation under stress (ca. 1%). This limited chain mobility also displays high deformation recovery by returning to nearly the original dimension after 20 minutes of relaxation. At higher loadings of the mono-oxetane (60O-40E), the material exhibits a twofold increase in elongation under stress due to the reduction in cross-link density in the cationic domain. Additionally, since the material contains greater degrees of phase separation, the continuous and more linear EHOX-EEC phase allows additional chain mobility. This trend in creep behavior is continued for the 75O-25E formulation which elongates to over 5% and corresponds to a nearly threefold increase in maximum elongation relative to 60O-40E. Furthermore, this more phase separated system exhibits less recovery and only recovers 80% of the maximum deformation. These results ultimately show that relative domain size scales and individual phase mechanical properties dictate macroscopic creep behavior of hybrid systems.

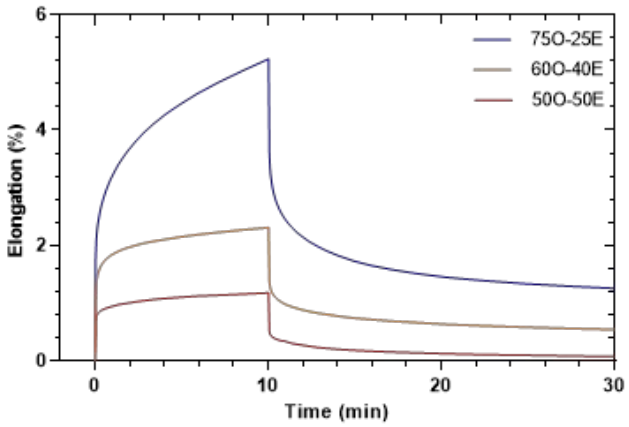

Figure 5. Creep testing of hybrid photopolymers with varied ratios of the cationic comonomers. Samples were subjected to sudden and constant pressure of 10 MPa, and this pressure was released after 10 minutes. All formulations contained 60 wt% free-radical and 40 wt% cationic polymerizable monomers. Samples were fabricated by polymerizing liquid formulation between two glass slides using a 405 nm LED at 20 mW/cm^2 for 5 minutes and then thermally post cured at 150 ˚C for 1 hour. Experiments were conducted at 25 ºC.

Depending on phase morphology, significant differences in deformation behavior of hybrid networks are possible. Therefore, these structural changes should also translate to a considerable impact on tensile properties. The stress/strain behavior of hybrid networks is shown in Figure 6A, and tensile properties are summarized in Table 2. When no epoxide is present in the system (100O-0E), very little mechanical resiliency is observed. The material displays a relatively low modulus, accompanied by low ultimate elongation and tensile strength. This behavior is consistent with the tan δ and phase morphology studies in that the bulk structure is highly phase separated. The soft, more continuous phase is composed of linear oxetane polymer and provides low structural integrity to the system. Moreover, continuity of cross-linking in the methacrylate domain is hindered by the large magnitude phase separation which further reduces bulk material stiffness. These structural features produce a material that is not able to withstand substantial stress loading or deformation and is thus prone to fracture. On the other hand, when only epoxide is present in the system (0O-100E), the material is very stiff with a tensile modulus that is over forty times greater than the 100O-0E. Additionally, 0O-100E displays a twenty-fold increase in tensile strength, but maximum elongation is significantly reduced. At this composition, the morphology is relatively homogenous with highly intertwined networks that inherently contain greater physical connectivity. Also, both domains contain high degrees of cross-linking which restricts translational movement to an even greater extent that manifests through low elongation.

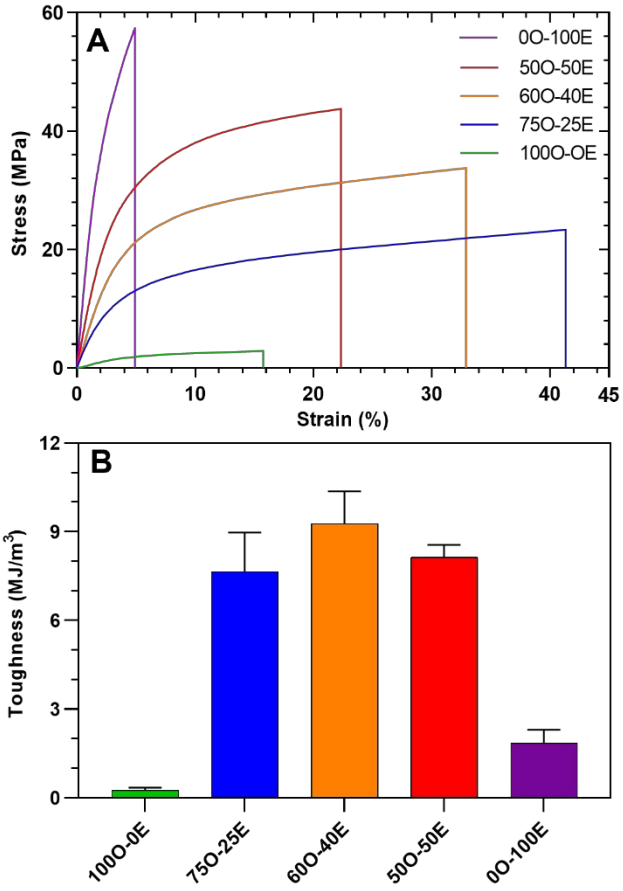

Figure 6A-B. (A) Representative stress/strain curves for hybrid formulations with either EHOX or EEC cationic monomers and intermediate mixtures of the two. (B) Tensile toughness for hybrid formulations. All formulations contained 60 wt% free-radical and 40 wt% cationic polymerizable monomers. Samples were stressed at a constant force rate of 2 N/m until failure. Samples were photopolymerized using a 405 nm LED at 20 mW/cm^2 for 5 minutes and thermal post cured at 150 ˚C for 1 hour. Experiments were conducted at 25 ºC.

Table 2. Tensile properties for hybrid photopolymer systems with changing ratios of cationic comonomers[a]

	Tensile Modulus (MPa)	Ult. Strength (MPa)	Ult. Elongation (%)	Toughness (MJ/m^3)
0O-100E	2200 (±100)	57.0 (±6.0)	5.0 (±0.8)	1.8 (±0.4)
50O-50E	1100 (±40)	44.1 (±0.5)	22.8 (±0.7)	8.1 (±0.4)
60O-40E	620 (±60)	33.6 (±1.2)	34.4 (±2.8)	9.2 (±1.1)
75O-25E	460 (±20)	23.6 (±1.3)	41.4 (±5.8)	7.6 (±1.3)
100O-0E	50 (±4)	2.7 (±0.3)	13.1 (±3.1)	0.26 (±0.1)

[a] Testing was performed in triplicate for each formulation and the reported values represent the mean ± standard deviation.

Vastly different tensile properties are demonstrated when comparing the extremes (i.e., highly phase separated to nearly full IPN structure). However, the greatest augmentation in mechanical robustness comes when balancing phase separation with domain interconnectivity to produce intermediate morphologies. As shown in Figure 6A, accelerating the EHOX polymerization with EEC

results in substantial property enhancements relative to the single cationic component formulations. The mixture with the lowest epoxide content (75O-25E) exhibits a 700% tensile strength increase, and elongation is possible over a much broader range (> 40% strain) relative to the 100O-0E formulation. These differences indicate much greater integration of the two domains from the enhanced polymerization rate and increased cross-linking in the EHOX-EEC phase. Moreover, with this significant integration between the stiff and flexible domains, toughness is markedly increased from 0.26 to 7.6 MJ/m^3 (+2800%). Increasing the epoxide content further to 60O-40E results in a 50% greater tensile modulus and strength relative to the 75O-25E but reduces ultimate elongation at failure to approximately 30%. At this concentration, the EHOX-EEC phase is no longer continuous (See Fig. 4) and long-range translational motion is extensively inhibited compared to the 75O-25E material. The amplified cross-linking in the EHOX-EEC domain and decreased phase separation between the networks increases the ultimate tensile strength of the material. This trend is continued at higher loadings of epoxide by imparting greater tensile strength while reducing elongation. Hence, as the EHOX-EEC network evolves at a faster rate and incorporates greater cross-linking, interpenetration between domains becomes prevalent and the global structure becomes more rigid. Compared to the IPN-like and highly phase separated structures (0O-100E and 100O-0E, respectively), material toughness for the formulations containing both EHOX and EEC exhibit an average eight-fold increase as shown in Figure 6B.

Interestingly, materials with different ratios of EHOX to EEC exhibit similar toughness values despite the large variations in stress/strain behavior. The results in Figure 6 show that modulus, tensile strength, and elongation can be modulated while maintaining overall toughness. By manipulating phase separated morphology, independent phases can impart higher modulus and/or higher elongation within the bulk material. Additionally, balancing phase separation with domain interconnectivity is essential to maintain structural stability. These findings establish that control over polymer morphology through

kinetics and monomer structure can allow tailored bulk mechanical properties in hybrid photopolymer systems.

To demonstrate the utility of internal control over phase separation in 3D constructs, the 75O-25E and 50O-50E hybrid systems were implemented using stereolithography. These formulations were selected since they exhibited the widest range in phase morphology while displaying similar tensile toughness. External processing parameters such as initiating light intensity, which has been shown to have a large influence on controlled phase separation,[21] are often limited in additive manufacturing. Therefore, the ability to control polymer structure and morphology independent of these processing factors enhances the versatility of 3D photopolymerization. Figure 7A shows the resin cure depth as a function of light dose for the 75O-25E and 50O-50E formulations. Linearizing these plots yields curing models for the photobleaching resins with a slope related to the light attenuation of the resin and an x-intercept indicative of the energy needed to reach gelation at the resin surface.[39] These models allow for quantitative comparison of curing characteristics between formulations and can be used to calculate the light dose required to cure a desired layer thickness. As expected, the penetration depth does not significantly change as the photo-active species concentration is the same with both formulations. Additionally, very little difference is evident between the energy to reach gelation between 75O-25E (59 mJ/cm^2) and 50O-50E (64 mJ/cm^2) ultimately showing that materials exhibiting a wide range of phase morphology can be printed independent of processing parameters.

With these similar curing parameters, identical print settings (e.g., layer thickness and layer exposure dose) were used to 3D print Izod impact blocks with the 75O-25E and 50O-50E formulations. Figure 7B shows images of the 3D printed blocks and the difference in optical characteristics between the two materials. The 75O-25E is opaque which is a result of the larger size scale of phase separation that reduces transmission of visible light.[34] The 50O-50E exhibits greater transparency due to greater entanglements between the two networks that reduces individual domain

size and interaction with light. The impact strength of these printed objects is shown in Figure 7C. Interestingly, the 50O-50E shows a nearly twofold increase in impact strength relative to the 75O-25E. Within layer-by-layer fabrication such as stereolithography, impact strength is dependent on bulk mechanical properties in combination with connectivity across the layer interface. Considering bulk mechanical properties, an argument could be made that the higher tensile modulus with similar tensile toughness (Fig. 6A and Table 2) balances structural rigidity with energy absorption permitting greater impact strength. However, the surface morphology at the layer interface also plays an important role in interlayer adhesion and ultimately impact strength of the 3D printed construct. The surface morphology of these two materials varies widely because of differences in phase separation and may influence bonding between layer laminations. Since the orthogonal polymerizations occur more simultaneously in the 50O-50E formulation, the resulting morphology contains less phase separation with a smaller surface dispersity of chemical composition relative to 75O-25E. The more homogenous dispersity of domains enables greater probability for similar domains to interact and covalently bond across the interface. Therefore, smaller and more integrated domains imparted by similar reaction kinetics in hybrid systems provides superior interlayer adhesion that manifests through increased impact resistance of 3D printed objects.

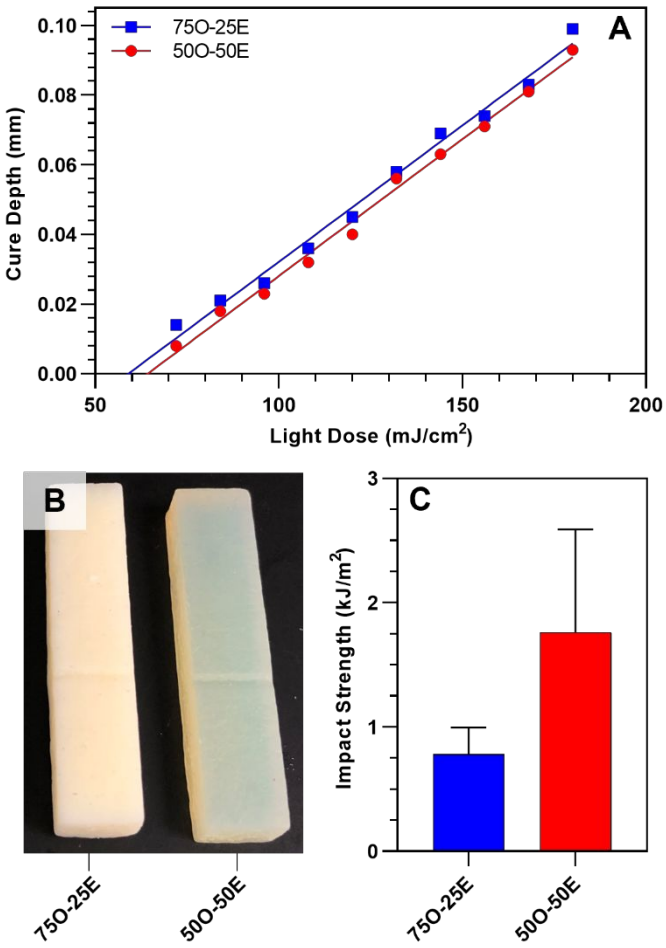

Figure 7A-C. (A) Photopolymer cure depth as a function of incident light dose (stereolithography working curve) for selected hybrid formulations: 50O-50E (red) and 75O-25E (blue). An array of squares was printed using stereolithography with each square receiving an increasing light dose. Individual square thickness was measured and plotted against the corresponding dose to construct the model. (B) Images of 3D-printed Izod impact test specimens for select formulations showing the large contrast in material opacity due to domain size/extent of phase separation. Printed objects consist of 300, 25 µm layers exposed for 8 s/layer with a 405 nm LED at 20 mW/cm^2. (C) Izod impact strength of the 3D-printed hybrid photopolymers. Samples were tested subjected to a 1 J pendulum hammer.

4 Conclusion

In this work, the effects of the oxetane/epoxide comonomer ratio on cationic photopolymerization kinetics, phase separation, and bulk material properties were examined in a hybrid photopolymer system. The system consisted of 60 wt% free-radical and 40 wt% cationic polymerizable monomers while the cationic comonomer ratio of a mono-oxetane (EHOX) to a di-epoxide (EEC) was altered. Without epoxide, the orthogonal polymerizations demonstrated vastly different reaction

kinetics with the free-radical monomers polymerizing within a few seconds under illumination while very little cationic polymerization occurred even after multiple minutes of light exposure. Inclusion of epoxide comonomer reduced the cationic induction period and increased polymerization rate. As a result, differences in the rate of formations for the two orthogonal networks were reduced resulting in the polymerizations occurring on similar time scales. Most importantly, the onset in cationic polymerization was controlled through adjustments in the oxetane/epoxide comonomer which enabled control over the magnitude of phase separation. For example, at low epoxide concentrations, materials exhibited dual tan δ maxima and discontinuous morphology as determined by DMA and AFM, respectively, indicating two localized areas of vastly different structural composition. Conversely, a single tan δ maximum and co-continuous phases were observed upon increasing the epoxide content. More pronounced dual phase morphology provided enhanced flexibility and elongation while greater network interpenetration increased stiffness and ultimate tensile strength. Thereby, tensile behavior was significantly modified without sacrificing polymer toughness. Furthermore, hybrid systems with controllable phase separation were fabricated using stereolithography to examine the effects of dual phase materials in 3D printing. Processing parameters were unaffected by resin formulation and domain morphology, although smaller domain size led to improved impact strength of 3D constructs, potentially through improved interlayer adhesion. This work on hybrid photocurable systems illustrates that control over phase separation, network structure and morphology can be employed to tune and improve photopolymer mechanical performance in thin film and 3D printing applications.

5 Acknowledgements

The authors would like to thank the Industry/University Cooperative Research Center (IUCRC) for Photopolymerization Fundamentals and Applications and the National Science Foundation (CBET-1438486) for support of this work.

6 References

1 Chatani, S.; Kloxin, C. J.; Bowman, C. N. The Power of Light in Polymer Science: Photochemical Processes to Manipulate Polymer Formation, Structure, and Properties. *Polym. Chem.* **2014**, *5* (7), 2187–2201. https://doi.org/10.1039/C3PY01334K.

2 Khudyakov, I. V. Fast Photopolymerization of Acrylate Coatings: Achievements and Problems. *Prog. Org. Coat.* **2018**, *121*, 151–159. https://doi.org/10.1016/j.porgcoat.2018.04.030.

3 Ifkovits, J. L.; Burdick, J. A. Review: Photopolymerizable and Degradable Biomaterials for Tissue Engineering Applications. *Tissue Eng.* **2007**, *13* (10), 2369–2385. https://doi.org/10.1089/ten.2007.0093.

4 Ligon-Auer, S. C.; Liska, R.; Stampfl, J.; Gurr, M.; Mulhaupt, Rolf. Polymers for 3D Printing and Customized Additive Manufacturing. *Chem. Rev. (Washington, DC, U. S.)* **2017**, *117*, 10212–10290.

5 Ligon-Auer, S. C.; Schwentenwein, M.; Gorsche, C.; Stampfl, J.; Liska, R. Toughening of Photo-Curable Polymer Networks: A Review. *Polym. Chem.* **2016**, *7* (2), 257–286.

6 Brett, C. J.; Montani, S.; Schwartzkopf, M.; van Benthem, R. A. T. M.; Jansen, J. F. G. A.; Griffini, G.; Roth, S. V.; Johansson, M. K. G. Revealing Structural Evolution Occurring from Photo-Initiated Polymer Network Formation. *Commun. Chem.* **2020**, *3* (1), 88. https://doi.org/10.1038/s42004-020-0335-9.

7 Gorsche, C.; Seidler, K.; Knaack, P.; Dorfinger, P.; Koch, T.; Stampfl, J.; Moszner, N.; Liska, R. Rapid Formation of Regulated Methacrylate Networks Yielding Tough Materials for Lithography-Based 3D Printing. *Polym. Chem.* **2016**, *7* (11), 2009–2014. https://doi.org/10.1039/C5PY02009C.

8 Jennings, J.; Green, B.; Mann, T. J.; Guymon, C. A.; Mahanthappa, M. K. Nanoporous Polymer Networks Templated by Gemini Surfactant Lyotropic Liquid Crystals. *Chem. Mater.* **2018**, *30* (1), 185–196. https://doi.org/10.1021/acs.chemmater.7b04183.

9 McLaughlin, J. R.; Abbott, N. L.; Guymon, C. A. Responsive Superabsorbent Hydrogels via Photopolymerization in Lyotropic Liquid Crystal Templates. *Polymer* **2018**, *142*, 119–126. https://doi.org/10.1016/j.polymer.2018.03.016.

10 Gorsche, C.; Koch, T.; Moszner, N.; Liska, R. Exploring the Benefits of β-Allyl Sulfones for More Homogeneous Dimethacrylate Photopolymer Networks. *Polym. Chem.* **2015**, *6* (11), 2038–2047. https://doi.org/10.1039/C4PY01582G.

11 Rong, M. Z.; Zhang, M. Q.; Ruan, W. H. Surface Modification of Nanoscale Fillers for Improving Properties of Polymer Nanocomposites: A Review. *Mater. Sci. Technol.* **2006**, *22* (7), 787–796. https://doi.org/10.1179/174328406X101247.

12 Owusu-Adom, K.; Schall, J.; Guymon, C. A. Photopolymerization Behavior of Thiol−Acrylate Monomers in Clay Nanocomposites. *Macromolecules* **2009**, *42* (9), 3275–3284. https://doi.org/10.1021/ma802656x.

13 Dean, K.; Cook, W. D. Effect of Curing Sequence on the Photopolymerization and Thermal Curing Kinetics of Dimethacrylate/Epoxy Interpenetrating Polymer Networks. *Macromolecules* **2002**, *35* (21), 7942–7954. https://doi.org/10.1021/ma020628p.

14 Jin, K.; Wilmot, N.; Heath, W. H.; Torkelson, J. M. Phase-Separated Thiol–Epoxy–Acrylate Hybrid Polymer Networks with Controlled Cross-Link Density Synthesized by Simultaneous Thiol–Acrylate and Thiol–Epoxy Click Reactions. *Macromolecules* **2016**, *49* (11), 4115–4123. https://doi.org/10.1021/acs.macromol.6b00141.

15 Dhulst, E. A.; Heath, W. H.; Torkelson, J. M. Hybrid Thiol-Acrylate-Epoxy Polymer Networks: Comparison of One-Pot Synthesis with Sequential Reactions and Shape Memory Properties. *Polymer* **2016**, *96*, 198–204. https://doi.org/10.1016/j.polymer.2016.04.032.

16 Zhao, T.; Yu, R.; Li, X.; Zhang, Y.; Yang, X.; Zhao, X.; Huang, W. A Comparative Study on 3D Printed Silicone-Epoxy/Acrylate Hybrid Polymers via Pure Photopolymerization and Dual-Curing Mechanisms. *J. Mater. Sci.* **2019**, *54* (6), 5101–5111. https://doi.org/10.1007/s10853-018-3070-1.
17 Karasu, F.; Rocco, C.; Lecompère, M.; Croutxé-Barghorn, C.; Allonas, X.; Zhang, Y.; Esteves, A. C. C.; van der Ven, L. G. J.; van Benthem, R. A. T. M.; de With, G. Influence of Actinic Wavelength on Properties of Light-Cured Interpenetrating Polymer Networks. *J. Polym. Sci. Part A: Polym. Chem.* **2016**, *54* (10), 1378–1390. https://doi.org/10.1002/pola.27988.
18 Szczepanski, C. R.; Pfeifer, C. S.; Stansbury, J. W. A New Approach to Network Heterogeneity: Polymerization Induced Phase Separation in Photo-Initiated, Free-Radical Methacrylic Systems. *Polymer* **2012**, *53* (21), 4694–4701. https://doi.org/10.1016/j.polymer.2012.08.010.
19 Szczepanski, C. R.; Stansbury, J. W. Accessing Photo-Based Morphological Control in Phase-Separated, Cross-Linked Networks through Delayed Gelation. *Eur. Polym. J.* **2015**, *67*, 314–325. https://doi.org/10.1016/j.eurpolymj.2015.04.006.
20 Williams, R. J. J.; Rozenberg, B. A.; Pascault, J. P. Reaction-Induced Phase Separation in Modified Thermosetting Polymers. In *Polymer Analysis Polymer Physics*; Advances in Polymer Science; Springer, 1997; Vol. 128, pp 95–156.
21 Hasa, E.; Scholte, J. P.; Jessop, J. L. P.; Stansbury, J. W.; Guymon, C. A. Kinetically Controlled Photoinduced Phase Separation for Hybrid Radical/Cationic Systems. *Macromolecules* **2019**, *52* (8), 2975–2986. https://doi.org/10.1021/acs.macromol.9b00177.
22 Inoue, T. Reaction-Induced Phase Separation in Polymer Blends. *Prog. Polym. Sci.* **1995**, *20*, 119–153.
23 Ge, X.; Ye, Q.; Song, L.; Misra, A.; Spencer, P. Visible-Light Initiated Free-Radical/Cationic Ring-Opening Hybrid Photopolymerization of Methacrylate/Epoxy: Polymerization Kinetics, Crosslinking Structure, and Dynamic Mechanical Properties. *Macromol. Chem. Phys.* **2015**, *216* (8), 856–872. https://doi.org/10.1002/macp.201400506.
24 Rocco, C.; Karasu, F.; Croutxé-Barghorn, C.; Allonas, X.; Lecompère, M.; Riess, G.; Zhang, Y.; Esteves, A. C. C.; van der Ven, L. G. J.; van Benthem, R. A. T. M.; de With, G. Highly-Interpenetrated and Phase-Separated UV-Cured Interpenetrating Methacrylate–Epoxide Polymer Networks: Influence of the Composition on Properties and Microstructure. *Mater. Today Commun.* **2016**, *6*, 17–27. https://doi.org/10.1016/j.mtcomm.2015.11.004.
25 Schissel, S. M.; Jessop, J. L. P. Enhancing Epoxide Kinetics and Tuning Polymer Properties Using Hydroxyl-Containing (Meth)Acrylates in Hybrid Photopolymerizations. *Polymer* **2019**, *161*, 78–91. https://doi.org/10.1016/j.polymer.2018.12.010.
26 Crivello, J. V. "Kick-Starting" Oxetane Photopolymerizations. *J. Polym. Sci. Part A: Polym. Chem.* **2014**, *52* (20), 2934–2946. https://doi.org/10.1002/pola.27329.
27 Bulut, U.; Crivello, J. V. Reactivity of Oxetane Monomers in Photoinitiated Cationic Polymerization. *J. Polym. Sci. A Polym. Chem.* **2005**, *43* (15), 3205–3220. https://doi.org/10.1002/pola.20723.
28 Sangermano, M.; Malucelli, G.; Bongiovanni, R.; Priola, A. Photopolymerization of Oxetane Based Systems. *Eur. Polym. J.* **2004**, *40* (2), 353–358. https://doi.org/10.1016/j.eurpolymj.2003.09.026.
29 Udagawa, A.; Sakurai, F.; Takahashi, T. In Situ Study of Photopolymerization by Fourier Transform Infrared Spectroscopy. *J. Appl. Polym. Sci.* **1991**, *42* (7), 1861–1867. https://doi.org/10.1002/app.1991.070420707.
30 Scholte, J. P.; Ki Kim, S.; Lester, C. L.; Guymon, C. A. Effects of Directed Architecture in Epoxy Functionalized Prepolymers for Photocurable Thin Films. *J. Polym. Sci. Part A: Polym. Chem.* **2017**, *55* (1), 144–154. https://doi.org/10.1002/pola.28377.

31 Green, B. J.; Guymon, C. A. Modification of Mechanical Properties and Resolution of Printed Stereolithographic Objects through RAFT Agent Incorporation. *Addit. Manuf.* **2019**, *27*, 20–31. https://doi.org/10.1016/j.addma.2019.02.008.

32 Škola, O.; Jašúrek, B.; Veselý, D.; Němec, P. Mechanical Properties of Polymer Layers Fabricated via Hybrid Free Radical-Cationic Polymerization of Acrylate, Epoxide, and Oxetane Binders. *Prog. Org. Coat.* **2016**, *101*, 279–287.

33 Decker, C.; Nguyen Thi Viet, T.; Decker, D.; Weber-Koehl, E. UV-Radiation Curing of Acrylate/Epoxide Systems. *Polymer* **2001**, *42* (13), 5531–5541. https://doi.org/10.1016/S0032-3861(01)00065-9.

34 Leguizamon, S. C.; Powers, J.; Ahn, J.; Dickens, S.; Lee, S.; Jones, B. H. Polymerization-Induced Phase Separation in Rubber-Toughened Amine-Cured Epoxy Resins: Tuning Morphology from the Nano- to Macro-Scale. *Macromolecules* **2021**, *54* (17), 7796–7807. https://doi.org/10.1021/acs.macromol.1c01208.

35 Scherzer, T.; Decker, U. The Effect of Temperature on the Kinetics of Diacrylate Photopolymerizations Studied by Real-Time FTIR Spectroscopy. *Polymer* **2000**, *41* (21), 7681–7690. https://doi.org/10.1016/S0032-3861(00)00141-5.

36 Franck, A. *Viscoelasticity and Dynamic Mechanical Testing*. TA Instruments. https://www.tainstruments.com/pdf/literature/AAN004_Viscoelasticity_and_DMA.pdf (accessed 2021-05-20).

37 Salmerón Sánchez, M.; Molina Mateo, J.; Romero Colomer, F. J.; Gómez Ribelles, J. L. Nanoindentation and Tapping Mode AFM Study of Phase Separation in Poly(Ethyl Acrylate-Co-Hydroxyethyl Methacrylate) Copolymer Networks. *Eur. Polym. J.* **2006**, *42* (6), 1378–1383. https://doi.org/10.1016/j.eurpolymj.2005.12.018.

38 Yu, R.; Yang, X.; Zhang, Y.; Zhao, X.; Wu, X.; Zhao, T.; Zhao, Y.; Huang, W. Three-Dimensional Printing of Shape Memory Composites with Epoxy-Acrylate Hybrid Photopolymer. *ACS Appl. Mater. Interfaces* **2017**, *9* (2), 1820–1829. https://doi.org/10.1021/acsami.6b13531.

39 Bennett, J. Measuring UV Curing Parameters of Commercial Photopolymers Used in Additive Manufacturing. *Addit. Manuf.* **2017**, *18*, 203–212. https://doi.org/10.1016/j.addma.2017.10.009.